JOURNAL OF GUIDANCE, CONTROL, AND DYNAMICS
Vol. 22, No. 2, March–April 1999

On-Orbit Closed-Loop Control Results for the Middeck Active Control Experiment

Mark E. Campbell*
University of Washington, Seattle, Washington 98195
Jonathan P. How†
Stanford University, Stanford, California 94305
Simon C. O. Grocott‡
SPAR Space Systems, Brampton, Ontario L6S 4J3, Canada
and
David W. Miller§
Massachusetts Institute of Technology, Cambridge, Massachusetts 02139

An in-depth analysis is presented of the closed-loop results and insights from the on-orbit control experiments of the Middeck Active Control Experiment (MACE). MACE was flown in the Shuttle middeck on STS-67 in March 1995 to investigate issues associated with a change in operational environment from ground to space for a payload pointing spacecraft that cannot be tested in a realistic ground simulation. These results show 1) equivalent performance can be obtained using finite element-based and measurement-based control design models; 2) the benefits available from testing the structure on the ground prior to flight, even if these tests are in a different configuration than that used on orbit; and 3) the performance limitations associated with various control topologies. These closed-loop results provide insight into how future on-orbit closed-loop experiments could be improved, and they also help build confidence in the on-orbit capabilities of future multipayload spacecraft.

I. Introduction

PRACTICAL control design for flexible systems involves many issues such as the selection of effective control topologies (sensor/actuator architecture), validation of robust control designs and techniques, development of robust control design methodologies for both finite element and identified models, and development of effective tools for system analysis. The Middeck Active Control Experiment (MACE) has been designed to be a reusable dynamics and control laboratory that can be used to investigate many of these issues during both ground- and space-based operations. This paper presents an in-depth analysis of the extensive set of (modeling and) closed-loop control experiments performed on the MACE test article during 14 days of on-orbit operations on STS-67 in March 1995.

In the past, control system performance has been limited by flexibility in the system due to a phenomenon known as control–structures interaction (CSI). CSI occurs when control detrimentally interacts with flexibility in a system, usually caused by mismodeling or lack of consideration of flexibility. One of the typical solutions to the CSI problem on spacecraft has been to analyze the system dynamics and limit the bandwidth of the control so that it does not include this flexibility. Therefore, flexibility has typically placed a limit on the performance of systems, particularly in space, where rigidizing the structure is obtained at high launch cost. In addition, many CSI problems are not identified until after the system has already been placed in operation, thus limiting possible solutions to operational workarounds. Overcoming this problem is accomplished by controlling rather than avoiding flexibility, requiring a multidisciplinary approach that combines state-of-the-art capabilities in modeling and model updating, system identification, uncertainty model development, linear systems analysis, and robust control synthesis. This approach is called controlled-structures technology (CST). The MACE program has been instrumental in streamlining and validating many of these CST tools so that they are sufficiently mature to be used reliably and predictably in real-world systems, including spacecraft in 0 g.

Although there have been several studies of practical control of flexible systems[1–4] and a very large number of CSI test facilities,[5,6] the MACE program is unique in its extensive implementation of on-orbit experiments. The program objective of MACE was to develop a set of CST tools that increase confidence in the eventual on-orbit performance of future spacecraft that cannot be dynamically tested on the ground in a sufficiently realistic 0-g simulation. The primary control objectives of the MACE flight were to demonstrate robust control of structural flexibility in the microgravity environment and to augment controllers designed prior to flight with on-orbit system identification and control redesign. Reference 7 presents an analysis of the overall flight results for MACE from a programmatic perspective. In particular, that paper outlines the five major objectives for MACE and how these were achieved. As a result, Ref. 7 covers a wide range of topics, including mission programmatics, testbed design, and highlights of the technical achievements in system modeling, identification, uncertainty modeling, and control design. In light of the mission summary in Ref. 7, this paper focuses on presenting a very detailed analysis of the closed-loop control results that were obtained on-orbit and compares them with predictions made prior to flight.

The main emphasis of this paper is to present a full comparison of the closed-loop performance that was achieved on two different configurations of MACE. These two configurations share many pieces of hardware, but only configuration I could be tested on the ground. The L shape of configuration II was selected so that there would be strong coupling with gravity and the suspension system. In this sense, configuration II was developed to be representative of the class of spacecraft that are difficult to test on the ground in a sufficiently realistic simulation. Thus, configuration II can viewed as the primary space structure for which good closed-loop performance is required. Configuration I corresponds to a simple, reasonably similar structure that could easily be tested on the ground. This change

Received Sept. 30, 1998; revision received Aug. 31, 1998; accepted for publication Sept. 2, 1998.

*Assistant Professor, Department of Aeronautics and Astronautics. Member AIAA.
†Assistant Professor, Department of Aeronautics and Astronautics. Member AIAA.
‡Intermediate Member of the Technical Staff.
§Principal Research Scientist, Space Engineering Research Center. Member AIAA.

to a different configuration provides a very strong test of the ability of the CST to model, predict, and account for significant variations in the system dynamics.

A secondary objective of this paper is to provide a summary of the extensive closed-loop results obtained on-orbit and, in the process, demonstrate the effectiveness and maturity of the CST tools that were developed for the MACE mission. In addition to the configuration I and configuration II results and comparison, several other aspects of the control design process and performance are explored using closed-loop results on configuration I.

The paper is organized as follows. The next section outlines the primary issues faced during the design of controllers for on-orbit operations. This is followed by several sections that discuss specific closed-loop experimental results obtained on-orbit, including an analysis of different configurations of the hardware, different control synthesis and analysis methods, different design models, and different sensor and actuator topologies. Only a very brief description of the MACE program is given, however, with more details available in Refs. 7 and 8.

II. Control Design Issues

Because of the unwavering support of the crew members on the STS-67 mission, over 400 controllers examining many different design issues (summarized in Table 1) were implemented during the 16-day flight. The following sections outline some of the most important control design issues that had to be addressed to achieve the overall program objectives.

A. System Configuration

The test article, shown in two configurations in Fig. 1, consists of a segmented flexible structural bus with integral power and data connections. The structure of the MACE test article was chosen to represent a precision-controlled, high payload mass fraction spacecraft, such as Earth observing platforms, with multiple, independently pointing or scanning payloads.[8] As such, there is a two-axes gimbaled payload containing a two-axes rate gyroscope for inertial pointing angle determination mounted at each end of the structural bus. A three-axes reaction wheel assembly (RWA) is mounted in the center to provide attitude control torques. A two-axes piezoelectric bending strut is located next to the RWA on the primary end of the structure. Each strut is instrumented with strain gauges measuring bending strain in two axes. An optical encoder is mounted on each gimbal axis to measure the angular displacement of the payload relative to the bus. The only difference between the two configurations is a 90-deg elbow node between struts 1 and 2. As will be seen, this small change created very large shifts in both the frequencies and mode shapes of the structure.

Configuration I in Fig. 1a was used to investigate the primary objectives of the MACE program, which were to compare the limits and predictability of performance achieved using both preprogrammed and redesigned controllers on a system that could be dynamically tested on the ground. It was tested for many months prior to flight

Table 1 Primary control design issues for MACE

Design issue	Approaches considered
System configuration	Configuration I, configuration II
Model fidelity	Finite element model (FEM) Measurement models (MM)
Robustness analysis	Data analysis, μ analysis
Uncertainty model	Parametric, data
Control design method	Classical, robust, narrow band, $\mathcal{H}_2/\mathcal{H}_\infty$
Control topology	Feedback performance variable z directly or not
Disturbance environment	Broadband, narrow band, step-stare

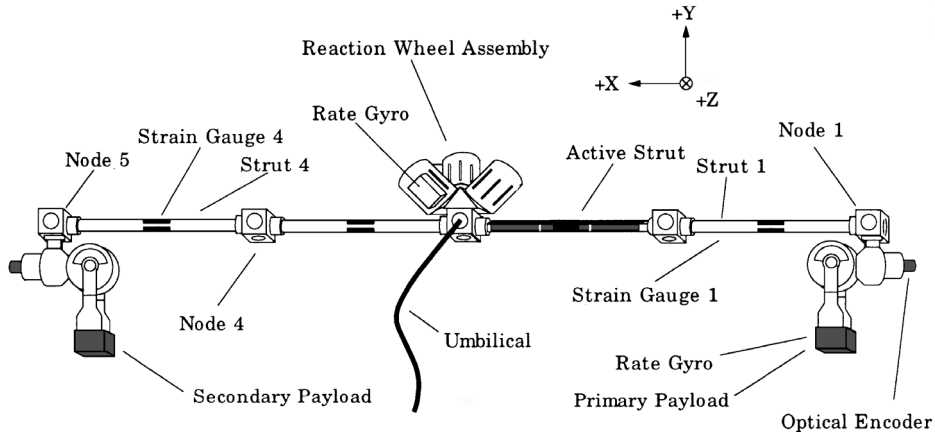

a) MACE configuration I

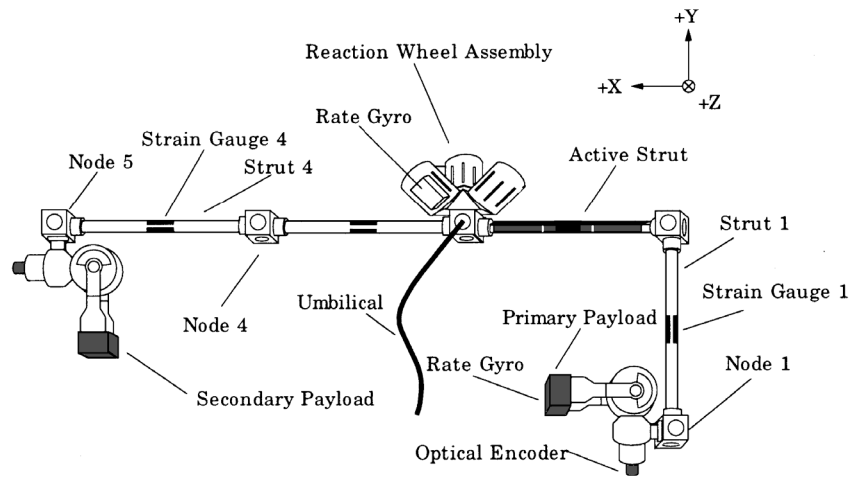

b) MACE configuration II

Fig. 1 MACE test article, 0-*g* configurations.

using a suspension system. Configuration II in Fig. 1b was used to demonstrate that lessons learned during ground tests with configuration I could be used to accurately predict the on-orbit performance for a different configuration. For this reason, and because large loads exerted by the gimbals on the bus structure significantly complicated ground testing, configuration II was not tested on the ground prior to flight. Note that the same modeling and control design procedures were used for both configurations.

The use of a second test article configuration is an important step in the analysis of closed-loop performance because many spacecraft cannot be tested on the ground in the same configuration that they will eventually be used on-orbit. Comparing performance achieved for the two configurations corresponds to an important new step in the modeling and control design procedure developed for MACE and other future spacecraft. In addition, this step has also not been accomplished with any of the other CSI ground facilities.

B. Model Fidelity

Attaining a high level of performance improvement in the pointing control of flexible systems requires not only an advanced control methodology, but also an accurate model of the dynamics. Two model types were used for MACE: 1) a high-fidelity finite element model[9] (FEM) developed and updated using insight from 1-g modeling and analytic predictions of the on-orbit dynamics and 2) a measurement model (MM) created using integrated frequency-domain observability range space extraction and least square parameter estimation technique[9] to obtain an extremely accurate fit of the data.

Two issues in the modeling process became very important during the Shuttle flight experiment. The first was several missing modes in the analytical model at low frequency. These low-frequency modes were caused by soft tethers, a necessary step used to position the test article in the Shuttle middeck, particularly during thruster firings. Application of tethers was at the discretion of the astronauts and, thus, could not be accurately modeled prior to flight. However, it was estimated that the frequency of the tether modes was lower than 0.01 Hz. As a result, tether modes were omitted from the 0-g analytical model, and authority of all controllers was designed to roll up only above 0.01 Hz. The umbilical, on the other hand, was included in the model, but unfortunately, in the wrong physical configuration. The model predicted the umbilical modes to be at 0.45 Hz, whereas the data showed that they were approximately 0.24 Hz; this difference did not substantially affect the designs. Whereas the measurement models were developed with the tethers in place, the analytic models were updated during the mission, using observations from the downlinked video, to include a more accurate representation of both the tether and umbilical modes.

As discussed in detail in Ref. 7, a second issue involved a slight amplitude nonlinearity in the system that proved to be a limiting factor in the control design. The nonlinearity was apparently caused by friction that locked the gimbals when the input excitation was quite small. The friction primarily changed the frequency and damping of modes in the 5–12 Hz frequency range. A detailed postflight analysis of this effect indicated that the system dynamics in closed loop were more accurately predicted in this frequency range by the FE model than by the MMs. This observation plays an important role in the closed-loop results to follow.

C. Robustness Analysis

Because of the uniqueness of the MACE experiment in implementing controllers in both 1 g and 0 g, two procedures were developed to analyze controllers for closed-loop stability and performance. An approach developed during the ground-based experiments, termed open-loop data analysis, is a quick and simple procedure that utilizes measured open-loop data. This approach works quite well if the open-loop data is available. However, the procedure could only be used for ground experiments and control redesigns during the mission, when data were available. Therefore, a second procedure was developed for those controllers designed prior to flight, termed a mixed-μ analysis.

The procedure for the open-loop data analysis is presented in Ref. 10 and summarized in the following. With open-loop data available in the form of a transfer function matrix

$$G(j\omega) = \begin{bmatrix} G_{zw}(j\omega) & G_{zu}(j\omega) \\ G_{yw}(j\omega) & G_{yu}(j\omega) \end{bmatrix} \tag{1}$$

where z are the performance outputs, y are the sensor outputs, w are the disturbance inputs, and u are the actuator inputs, we can close the loop using this data and the frequency response of the controller. The model and data predictions can then be overlaid to provide a prediction of the closed-loop performance, stability, and proximity to instability.

The system performance is analyzed using the closed-loop state cost,[11] whereas the closed-loop stability is assessed using two tests: the multivariable Nyquist test and the sensitivity transfer function. For absolute closed-loop stability, the number of counterclockwise encirclements of the critical point $(-1, 0)$ of the multivariable Nyquist function

$$H_n(j\omega) = -1 + \det[I + G_{yu}(j\omega)K(j\omega)] \tag{2}$$

must equal the number of unstable poles in the open-loop system and compensator. In a Single input/single output (SISO) system, the Nyquist function additionally provides measures of proximity to instability in the form of gain and phase margins. For multi-input/multi-output (MIMO) systems, however, the margins cannot be obtained from the Nyquist function. Instead, the maximum singular value of the sensitivity transfer function

$$\bar{\sigma}[S(j\omega)] = \bar{\sigma}\left\{[I + G_{yu}(j\omega)K(j\omega)]^{-1}\right\} \tag{3}$$

gives a direct measure of the proximity to singularity. For example, if model-based and data-based calculations of $\bar{\sigma}[S(j\omega)]$ strongly disagree, and $\bar{\sigma}[S(j\omega)] > 1$ for either case, then the controller is not robust to model errors and could possibly destabilize the actual system.

Prior to flight, open-loop 0-g data were not available, and so a different analysis method had to be used. For structural systems such as the MACE test article, the most significant model errors and uncertainties are typically in the frequency and damping of the flexible modes.[9] Therefore, an alternative method was developed[12,13] that uses a mixed-μ analysis along with a model of the parametric uncertainties to analyze the closed-loop system to check for stability and performance over the predicted range of uncertainty. For MACE, it was necessary to predict the frequency and damping uncertainties in 0 g based on 1-g testing, a procedure that is described in the following section.

The mixed-μ analysis[14,15] used an uncertainty set that included 20 real parametric uncertainties (frequencies and damping ratios of 10 modes) and one complex uncertainty to ensure the problem is continuous in the problem data.[14] Motivated by the open-loop data analysis, which indicated that significant variation between model and data predictions of $\sigma_i[S(j\omega)]$ correlated well with poor experimental robustness, the complex uncertainty block is a weighted (maximum singular value of the) sensitivity transfer function, which gives a measure of the proximity to instability of the closed-loop system. A scaling factor α determined the maximum allowable change in the perturbed sensitivity. Ground-based experimental tests indicated that $\alpha = 2$ led to good closed-loop stability and performance. As constructed, this μ test provides information very similar to the open-loop data analysis. However, because the μ analysis is based on the predicted uncertainty model rather than data, this approach could be used to analyze the controllers prior to flight. The full details of the μ analysis are discussed in Ref. 13.

D. Uncertainty Model

The open-loop data analysis procedure inherently contains a measure of the modeling uncertainty. It compares predicted stability and performance for both model and data, and the difference gives a qualitative measure of the modeling error, which is very useful for robust control design. The μ analysis, on the other hand, uses an uncertainty model in the form of predicted parameter variations for

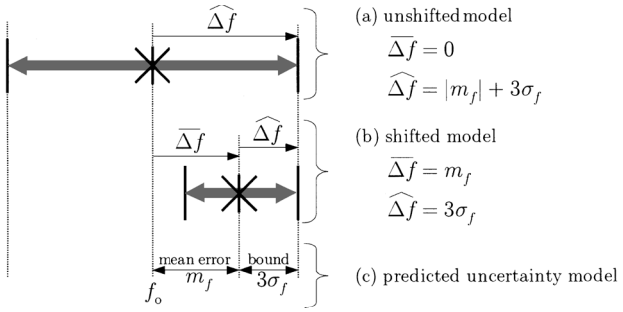

Fig. 2 Two primary uses of the uncertainty model for a sample FEM frequency f_0: a) unshifted FEM used for synthesis and large bounds scaled to cover the entire uncertainty model ($|m_f| + 3\sigma_f$) used for analysis and b) FEM shifted by the mean errors m_f used for synthesis and bounds $3\sigma_f$ used for analysis.

closed-loop analysis. A 1-g uncertainty model, in the form of mean and variance of parameters, was developed by measuring the difference in frequencies and damping ratios between several identified models and the FEM to provide a measure of the modeling error and the variability of the structure on the ground. The mean and variance of the 0-g structural parameters were then predicted using a method described in Ref. 12. The approach uses a perturbation expansion of the generalized structural eigenvalue problem to convert frequency mean and variance uncertainties to mass and stiffness perturbations. These physical uncertainties are then mapped into 0 g using the FEM to predict mean and variance errors for the on-orbit frequencies. Damping predictions are more tenuous and difficult to predict, and so the 0-g damping uncertainty model was simply a scaled version of the 1-g damping uncertainty model, which is obviously conservative.

Control design and analysis with μ utilized a single nominal design model, along with a range of parameter variations. There are several approaches to using the predicted 0-g uncertainty model in the μ framework, each with different levels of conservatism. Two approaches used for MACE are shown for a sample frequency f_0 in Fig. 2. The first, shown in Fig. 2a, used the 0-g FEM as the design model, and the predicted mean errors m_f and $3\sigma_f$ bounds for each parameter were combined into a large overbound for analysis ($|m_f| + 3\sigma_f$). This approach is the most conservative use of the uncertainty model, reflecting the low confidence in the uncertainty prediction prior to flight. A second approach, shown in Fig. 2b, shifted the 0-g FEM by the mean errors m_f of the uncertainty model to create a new control design model. If the mean errors are accurately predicted, then this model provides improved accuracy over the FEM. The predicted $3\sigma_f$ bounds reflecting variations about these means are then used for analysis. This second option results in less conservative controllers, but is appropriate only if confidence in the uncertainty model is high.

E. Control Design: Objective, Methods, and Procedure

Objective and Performance Definition

The specific objective of the control designs was to inertially point the primary precision pointing payload while the second scanning payload underwent broadband disturbance (0–50 Hz) or slew maneuvers. As such, the performance is defined as the two-axes pointing angle error of the primary payload, along with a small penalty on the motion of the center node, because a good control design should not only point the primary payload, but also not excite the bus. Specifically, the performance is defined as a combination (square root of the weighted sum of the signals squared) of all five integrated rate gyros, with a weighting 1 for the two in the primary payload and 0.1 for the three at the center node.

The most prevalent results discussed are for the two-axes disturbance rejection problem, where two independent white noise disturbances enter each axis of the secondary gimbal. The experimental spectral amplitudes of these disturbances were chosen such that 1) the sensors did not saturate in open loop and 2) the signal to noise ratio was large enough in closed loop. For this problem, a scalar performance metric is defined as the two-axes, root mean square pointing angle error between 0.5 and 50 Hz, for disturbance inputs with a scaled spectral amplitude of (1 deg)^2/Hz. In the frequency domain, this scalar rms is

$$\sigma_z = \left\{ 2 \int_{0.5}^{50} \mathrm{tr}[R_{zz} S_{zz}(f)]\, \mathrm{d}f \right\}^{\frac{1}{2}} \tag{4}$$

where z is a vector of five integrated rate gyros, R_{zz} is a diagonal matrix of weightings (1 or 0.1), and $S_{zz}(f)$ is the power spectral density of z. In subsequent plots, the square root of the integrand is plotted as a function of frequency (in degree per square root hertz). The quoted decibel reduction is the rms improvement of the performance metric in the 0.5–50 Hz range.

As a basis for comparing the CST control, local servocontrollers between the four encoders and their respective gimbal axes were used to define the open-loop system. A low-bandwidth servo (1/10th the frequency of the first flexible mode in each axis, 2.1 and 3.7 Hz) was used as standard industry practice for pointing control because it avoids interaction with the structural flexibility. Two layers of control were added from this open-loop case. First, the bandwidth of the servos was increased to approximately 2 Hz to perform nominal payload pointing with respect to the spacecraft bus. The overall pointing performance was then improved further by designing higher authority CST controllers that reduced the impact of the structural vibrations of the spacecraft bus.

Methods

Many different control techniques[10,16–20] were analyzed on the MACE test article prior to flight[10,11,21] and ranked in terms of three important criteria.

1) Conservatism in the performance/robustness trade off was determined. As discussed, the robust control designs typically included error models with 20 real parametric uncertainties. Thus, robust control techniques were tested to determine how much performance would be sacrificed to provide the required levels of parametric robustness.

2) Computational effort and degree of user input required during the design was rated. For fixed, ground-based experiments, computational requirements and the degree of user input required during the control design are typically not key parameters in the selection of a synthesis algorithm. However, for MACE it was required to redesign MIMO controllers in a 12-h period during the flight for implementing during the next mission day. This design cycle was repeated several times during the 14-day mission.

3) Performance during ground-based tests was ranked. Numerous ground-based experiments were used to compare predictability and effectiveness of the robust control techniques.

Together, these criteria were used to identify methods and a procedure suitable for designing parametric robust compensators for MACE. Here, the comparison and selection of the control design methods is summarized; a more detailed discussion is given in Ref. 10.

Four types of control design methods were used during the mission. The first method used a set of design rules for the synthesis of low-order robust MIMO controllers. These rules were developed by interpreting robust optimal designs in a classical manner, termed classically rationalized controllers.[21] The second method blended several robust $\mathcal{H}_2$ techniques to synthesize controllers. The third type of designs were developed for narrow-band disturbances using frequency-shaped $\mathcal{H}_2$ cost functionals. The final type of designs optimized a weighted $\mathcal{H}_\infty$ measure of the performance objective.

Because the $\mathcal{H}_2$ design approach demonstrated higher performance and robustness during ground testing, it was the tool most used of the four. As the name implies, this method blends three different techniques that optimize the overall $\mathcal{H}_2$ performance objective. These included linear quadratic Gaussian (LQG) controllers[22] and two robust $\mathcal{H}_2$ designs: sensitivity weighted LQG (SWLQG)[10,16] and multiple model techniques,[18] implemented in that order. Within this framework, the LQG design approach was used to identify key robustness issues using lower control authority designs, made easier by the closed-form solution that can be computed rapidly. The SWLQG technique was then used to determine

how best to account for these robustness problems, i.e., which parameters should be treated as uncertain, and in the process, increase control authority. Finally, the multiple model approach was used to push performance to the limits of controller authority. Ground tests using the multiple model technique showed that the approach, although only an approximation, provides a very good performance/robustness tradeoff (objective 1) and controllers performed very well on the test article (objective 3). In addition, using a numerical optimization discussed in detail in Ref. 18, the iteration time for these controllers was quite short (objective 2).

Procedure

For complicated systems such as MACE, good closed-loop performance requires a design procedure that systematically allows comparison and selection of a large number of performance, sensor, actuator, and noise weights. Furthermore, for robust control synthesis, there are many additional degrees of freedom, such as the selection of uncertain model parameters and robustness bounds. To complete these MIMO designs on a reasonable timescale (objective 2), the overall design problem was split into several independent control problems for particular parts of the structure.

1) Design independent SISO (X, Y, and Z axes) bus rate gyro to reaction wheel local loops.

2) Design independent SISO (X and Z axes) primary rate gyro to primary gimbal local loops.

These two steps were used to design initial component controllers to provide insight into issues associated with the more complex MIMO control synthesis, such as the determination of relative performance weights, actuator usage, and robustness requirements. The insights and results from these analyzes were then used to initialize the design of MIMO controllers.

3) Design each full XY (3×3) and Z (2×2) axes controllers with insights from steps 1 and 2.

4) Design the full XYZ (5×5) controller using insights from steps 1, 2, and 3.

The principle behind this methodology is that a better understanding of the effects of the design parameters and faster iteration time can be obtained by studying simpler problem subsets, rather than the whole set. During the MACE flight, each member of the control design team examined a particular component of the overall design (steps 1–3). The resulting information was then used to initialize the more complex MIMO designs (step 4). This uncoupled design philosophy provided many insights into robustness issues and control authority allocation and, as such, greatly improved the initialization of the MIMO control designs. It was a crucial factor in being able to produce enough MIMO controllers during flight that could be uploaded for the next mission day. A total of 180 multivariable controllers were redesigned and implemented during the first eight days of the mission.

A further procedural aspect of the control synthesis for MACE was that controllers were designed and grouped in families. Each family consisted of 1–8 control experiments that used the same control topology, design method, analysis method, model, and disturbance input. The members of the family only differed in control authority, which was increased from very low authority (highly likely to be stable) to high authority (predicted to have questionable stability or performance). For instance, a family of eight controllers designed with the $\mathcal{H}_2$ method would typically consist of (in order): two LQG controllers (low authority), three SWLQG controllers (medium authority, medium to high robustness), and three multiple model controllers (high authority, high robustness).

F. Control Topology

The MACE test article was also designed to investigate the impact of various sensor and actuator topologies on closed-loop performance. The nominal sensor/actuator suite consists of five inputs (two-axis primary gimbal and three-axis reaction wheels) and five outputs (two-axes rate gyros in the primary payload and three rate gyros at the center of the bus). With this suite, the derivative of the performance metric is part of the measured outputs (primary rate gyros). It is well known that feeding back the performance metric simplifies the control design immensely and allows very large performance improvement.[21] Several other sensor/actuator topologies were also investigated that did not feed back the performance metric to determine the impact of this type of constraint on the control design.

Table 2 Summary of MACE closed-loop results discussed

Section	Configuration	Model, analysis	Topology	Comment
III.A	C-I	FEM PP[a] FEM RD[b] MM RD[b]	PV[c]	C-I families
III.B	C-I	FEM PP[a]	PV[c] NPV[d]	Topology
III.C	C-I	FEM PP[a] SM PP[a]	PV[c]	SM
IV.A	C-II	FEM PP[a] FEM RD[b] MM RD[b]	PV[c]	C-II families
IV.B	C-I, C-II	FEM PP[a] FEM RD[b] MM RD[b]	PV[c]	C-I/C-II comparison

[a]Controllers using μ analysis/uncertainty model.
[b]Controllers using open-loop data analysis.
[c]Pointing performance z fed back.
[d]Pointing performance z not fed back.

G. Summary of MACE Closed-Loop Results Presented

Table 2 shows a summary of the MACE closed-loop results to be presented in the following two sections, as a function of the design issues discussed in this section. Section III.A compares three controllers for configuration I: FEM preprogrammed (PP), FEM redesigned (RD), and MM RD. Section III.B demonstrates how much performance can be attained when the performance variable (PV) is not fed back (NPV). Section III.C shows the benefits of using the shifted model (SM) for control design (SM PP, FEM PP). Section IV.A compares three controllers for configuration II: FEM PP, FEM RD, and MM RD. Finally, Sec. IV.B compares the results and lessons learned on both configurations I and II.

III. On-Orbit Configuration I Closed-Loop Experiments

The following sections discuss closed-loop control results from several stages of the MACE mission, including FEM- and MM-based designs, different control topologies, and the use of a shifted design model. All results shown are for the two-axes disturbance rejection problem described in Sec. II.E, where independent white noises enter each axis of the secondary gimbal. The scalar performance metric, the square root of the weighted sum of the five integrated rate gyros squared, is plotted. A decibel reduction is quoted to measure the rms improvement of the performance metric in the 0.5–50 Hz range. All controllers presented, except those in the topology section, used a nominal set of five actuators (three reaction wheels and two axes of the primary gimbal) and five sensors (rate gyros at the center of the bus and in the primary payload). In the figures presented (for example, see Figs. 3 and 4), open-loop refers to the system response with the low-bandwidth (industry standard) servos and servos only refers to servos designed with a bandwidth at approximately 2 Hz for each gimbal–encoder pair.

A. Configuration I Results

Configuration I was the system configuration that was most utilized during the MACE flight and is shown in Fig. 1a. During the first day of the mission, an identification of the dynamics of configuration I was performed, downlinked, and used to create measurement models. A family of PP controllers designed prior to flight using the FEM were then implemented, whereas controllers were redesigned using the FEM and MM and uplinked on the third day. Two additional MM redesigns were also implemented later in the mission.

The PP controllers were very dependent on the conservatism and accuracy of the uncertainty model. Table 3 shows a summary of the results for both the unshifted model and SM approaches to using the uncertainty model (explained in Fig. 2), along with the FEM frequencies. The Δf refers to a shift in the FEM to create the nominal

Table 3 Data showing the predicted 0-*g* uncertainty model for configuration I

		Uncertainty model 1		Uncertainty model 2		Data	
Mode type	f_{FEM}, Hz	$\overline{\Delta f}$, %	$\widehat{\Delta f}$, %	$\overline{\Delta f}$, %	$\widehat{\Delta f}$, %	$\overline{\Delta f}$, %	$\widehat{\Delta f}$, %
1st Vertical	2.26	0.0	4.7[a]	−1.5	3.2	3.8	4.1
1st Horizontal	3.73	0.0	8.1[a]	−4.3	3.8[a]	−2.9	4.6
2nd Horizontal	9.46	0.0	5.5[a]	3.6	1.9[a]	5.5	2.3
2nd Vertical	16.1	0.0	3.7[a]	1.4	2.3	−2.1	2.7
3rd Horizontal	17.8	0.0	1.4[a]	0.3	1.1	−1.4	0.2
4th Horizontal	25.0	0.0	1.6[a]	0.8	0.8[a]	−1.6	2.9
3rd Vertical	39.6	0.0	7.5[a]	−3.0	4.5[a]	−3.2	2.9
4th Vertical	49.2	0.0	5.6	−4.1	1.5	−9.0	2.0
5th Horizontal	49.7	0.0	5.0[a]	−2.1	2.9[a]	−2.5	2.3
6th Horizontal	57.0	0.0	4.8	−3.7	1.1	−12.8	3.2

[a]Mean data frequencies within predicted bounds.

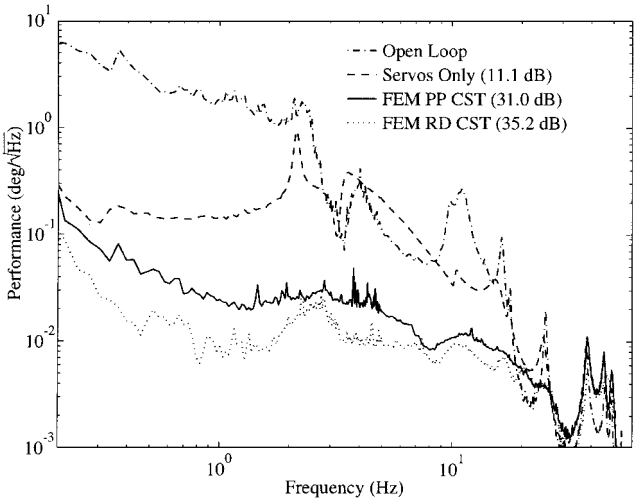

Fig. 3 On-orbit FEM based results for MACE configuration I; predicted uncertainty model and μ-analysis used to test for robustness.

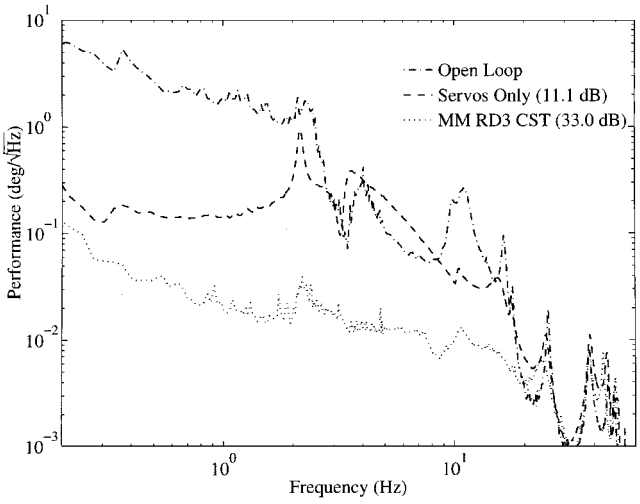

Fig. 4 On-orbit measurement model based results for MACE configuration I; open-loop data analysis used to test for robustness.

design model. For uncertainty model 1, the most common and conservative form, the FEM is used as the design model and is not shifted ($\overline{\Delta f} = 0$). For uncertainty model 2, the shift is nonzero indicating that the SM is used for design ($\overline{\Delta f} = m_f$). The $\widehat{\Delta f}$ refers to the variations in the modal frequency about the shifted mean value, used in both control design and analysis. The parameter variations for uncertainty model 1 are much larger than those for uncertainty model 2 because they combine the mean errors and $3\sigma_f$ bounds from the predicted uncertainty model ($\widehat{\Delta f} = |m_f| + 3\sigma_f$), whereas the variations from uncertainty model 2 only use the predicted bounds themselves ($\widehat{\Delta f} = 3\sigma_f$).

The superscript in Table 3 denotes those parameter variations that cover the actual frequencies of the system, according to the measured on-orbit data. For uncertainty model 1, 8 of 10 measured frequencies were covered by the predicted uncertainty model. Two high-frequency modes were not covered by the predictions, but because the controllers were designed to be very robust in this frequency range, these were not limiting factors in the on-orbit performance. Uncertainty model 2 was not as accurate, with the SM and variations covering only 5 of the 10 frequencies. However, the mean of the errors of the frequencies of the nominal design model was reduced from 4.6 to 3.1%.

Figure 3 shows the (open- and) closed-loop performance for the best XYZ results for configuration I. The scalar performance cost, which is the square root of a weighted sum of the five integrated rate gyros squared, is plotted. The solid line in Fig. 3 shows the best PP controller based on the FEM control design model. This controller, as with all FEM PP controllers, was analyzed using the predicted uncertainty model (see Table 3) and μ analysis. This particular controller was designed using the multiple model technique. A 31-dB (factor of 35) performance improvement was achieved over a broad frequency band, and the controller has significantly modified the dynamics up to approximately 30 Hz. The limiting factor in the PP designs was the unmodeled tether modes discussed in Sec. II.B. The dominant tether mode at approximately 0.14 Hz was destabilized by the next higher authority controller.

A family of FEM-based controllers were RD using the open-loop data analysis. In addition, a second-order shaping filter on the control effort was added that substantially increased the control penalty below 0.5 Hz to avoid interaction with the tether modes, while still achieving performance over the 0.5–50 Hz range. The best of these closed-loop results is shown in Fig. 3. The FEM RD controllers noticeably improved the performance up to 20 Hz, resulting in a 35.2-dB improvement (factor of 58). These controllers also provided more robustness to high-frequency model errors, as indicated by the sensitivity analysis (not shown). Because this is a pointing experiment, it is also important to evaluate the time-domain response for various disturbance commands. Time-domain analysis of this controller for broadband and step commands is given in Ref. 7, showing remarkable improvement. This performance improvement is also demonstrated in Fig. 5 with a narrow-band disturbance that consists of a sine wave at 3.65 Hz in the X direction and one at 2.10 Hz in the Z direction. As Fig. 5 clearly shows, the CST control provides a factor of 15–20 reduction in pointing error over the servoed system.

Controllers were also designed using the MM and were analyzed using open-loop data analysis (MM RD1–MM RD3). Because MMs are typically much more accurate than the FEM, robustness levels for these controllers were much smaller than those used for the FEM-based controllers. This approach resulted in many successful control designs during the extensive ground tests prior to flight. Figure 4 shows performance results using MM-based controllers (MM RD3), demonstrating significant broadband improvement in the pointing objective, corresponding to a 33-dB (factor of 45) improvement in performance. This surpasses the performance levels of the FEM PP controllers, but not the FEM RD controllers. This result is quite surprising because numerous ground tests indicated

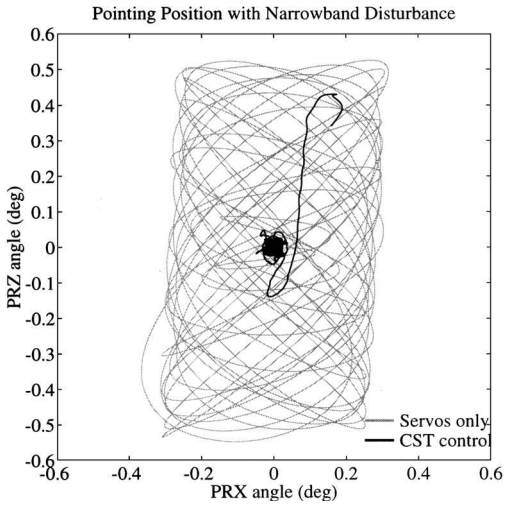

Fig. 5 Angular displacement trace of open- and closed-loop performance for narrow-band disturbance in each axis.

that control based on the identified models consistently gave better closed-loop performance than the FEM-based designs.[23]

The symptom of the difficulties experienced on-orbit was that the MM RD1 controllers drove the Z-axis dynamics unstable near 10 Hz. This was clear from the measured closed-loop data, but did not appear in the open-loop data analysis. A variety of methods were used to compensate for what apparently were differences between the measured/identified dynamics on the first day of operations and the test article dynamics on later days. One approach was to redesign controllers with significant amounts of robustness on three modes near 10 Hz. These attempts to robustify the compensators stabilized the system, but also limited performance improvement. A second approach was to use an additional set of open-loop data for control analysis, but this was not available until later in the mission.

A postflight comparison of three system identification tests taken at different input amplitudes and different points in the mission confirmed that changes occurred in the system response in this frequency range. This indicated that a previously unobserved stiction nonlinearity in the gimbals modified the boundary conditions of the structure and resulted in changes in the dynamics near 10 Hz (Refs. 9 and 13). Thus, the MM very accurately fit the measured data, but did not provide a good control design model for high-authority controllers because of the amplitude-dependent nonlinearity in the system. Furthermore, the postflight analysis demonstrated that the actual response of the system was more accurately represented by the FEM than by the MM. A complete summary of the issues associated with the nonlinearity is given in Refs. 9 and 13.

The performance results from the MACE flight for configuration I are succinctly summarized in Fig. 6. This plot compares the predicted ($\circ$) and actual ($\times$) closed-loop performance obtained by the MIMO compensators designed using the predicted (FEM) and measured (MM) dynamics and analyzed using μ for PP controllers and data analysis for RD controllers. Each curve corresponds to a family of compensators with increasing control authority (achieved by decreasing the control penalty and the sensor noise in the robust $\mathcal{H}_2$ design). The asterisk indicates that a second set of data was used in the open-loop data analysis procedure.

The FEM PP compensators were designed with increasing control authority until the μ analysis using the predicted 0-g uncertainty model indicated potential instability from a perturbation within the uncertainty set. In this case, the first four MIMO controllers were designed using SWLQG, and the remainder were designed using the multiple model technique. The closed-loop results show that performance improvement was predicted quite well, except for the last controller, which destabilized the low-frequency (0.14 Hz) tether mode. The presence of the tether mode and its gradual deterioration in performance were the primary cause for divergence in the prediction accuracy for the FEM PP family.

The FEM RD controllers included a shaping filter on the control effort, substantially increasing the control penalty below 0.5 Hz to avoid interaction with the tether modes. These controllers were designed using the multiple model technique and analyzed using open-loop data. Because the open-loop data analysis more accurately reflects the actual dynamics of the system and is less conservative than the uncertainty model/μ analysis, the FEM RD controllers extended the performance improvement to 35.2 dB (compared to the 31.0 dB of the FEM PP). The predicted performance matches the actual performance very well for all cases. The limiting factors in these designs were phase loss (due to the sensor dynamics and computational delay) and sensor noise.

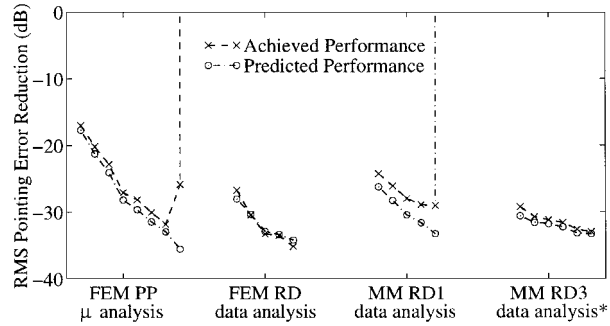

Fig. 6 Configuration I performance comparison.

The first MM controllers (MM RD1) did not fare as well. The predicted and actual performance diverged with increasing authority, with the final controller destabilized the system near 10 Hz. These poor predictions, caused by a deterioration in the stability and performance near 10 Hz, were the result of two factors. First, the MM was an excellent fit to the open-loop data, so that there were no significant deviations between the model and data predictions in either $H_n(j\omega)$ or $\bar{\sigma}[S(j\omega)]$. As a result, there was very little indication of how the controller should be robustified, and confidence from numerous ground tests gave little reason to expect any significant robustness issues. The second, more important, factor was the failure of the linear open-loop analysis to predict the problems at 10 Hz caused by the nonlinearity.

Several redesigns of the MM-based controllers were also performed. The MM RD3 controllers used the same model as the MM RD1 controllers but had the added benefit of a second set of measured open-loop data downloaded from the Shuttle for performance analysis. (Note that several operational and communication constraints limited our ability to obtain and download additional open-loop data. These factors, combined with the physical remoteness of the experiment, placed significant limitations on the analysis of the nonlinearity that could be performed during the mission.) As shown (Fig. 6), the predictions matched the actual results much better. In addition, the 10-Hz problem was addressed in the robust control designs to prevent destabilization of the actual system. The best achievable performance was increased to 33.0 dB (compared to the 28.9 dB of MM RD1). The performance levels, however, were still lower than those obtained with the FEM. This difference is attributed to both a lack of design heritage (9 months for FEM, 9 days for MM) and performance degradation associated with the conservative techniques used to avoid destabilizing the system at 10 Hz.

These results clearly indicate that the robust control design and analysis methods worked quite well for the FEM-based controllers. Of the 130 FEM PP configuration I controllers that were implemented, only seven destabilized the system. Of these seven, three were predicted to be unstable (designed using LQG), and the remaining four destabilized the low-frequency tether mode. Comparable performance was eventually achieved using the identified models, but model refinement and control redesign process were constrained by the limited amount of data that could be downlinked during the mission. The difficulties experienced with control designs based on the identified models illustrate the importance of further research in the fields of system identification and model unfalsification.[24,25]

B. Sensor/Actuator Topology

Tests were also conducted to study the impact of controller topology on the achievable performance. In particular, several controllers

were designed that did not feed back the rate gyros in the primary payload (the performance metric), as this is a topology that is known to be capable of higher performance, but is not always realistic.[21] Many different designs were attempted using a variety of actuators and sensors including strut strain gauges to measure the structural vibrations, bus rate gyros to provide bus orientation, and primary encoders to measure relative gimbal pointing angles. For these cases, the structural flexibility that exists between the measurements on the bus and the relative measurements at the gimbal typically plays a larger role in determining the feedback gains and, ultimately, the performance. Consequently, controllers for these topologies depend heavily on the system model and are often plagued with robustness concerns.[11]

Because of the hindered performance and robustness concerns caused by not feeding back the performance metric, two design decisions were made. First, the encoders appeared to be the best sensor in terms of achievable performance, primarily because of their relatively close location to the payload rate gyros. The use of encoders and bus rate gyros would allow the design to infer the inertial position of the gimbal. Second, to increase the robustness of the loops, a high-authority control/low-authority control (HAC/LAC)[26] architecture was employed. A low-authority controller consisting of two independent integral feedback controllers was closed between the two axes (X and Z) of the active strut and collocated strain gauge pairs. The LAC was designed to add stability robustness to the system by increasing damping in the 10-, 17-, and 25-Hz modes. These modes were targeted because the μ analysis indicated robustness problems may exist without this added damping. The HAC was based on a MIMO (five inputs and five outputs) robust multiple model controller using the primary gimbal and reaction wheel actuators and the primary encoders and bus rate gyro sensors. Note also that the HAC/LAC design was a PP controller, designed using the FEM, predicted uncertainty model, and μ analysis.

Figure 7 shows the best XYZ closed-loop results obtained using this HAC/LAC approach and not feeding back the performance metric (NPV), along with the best FEM PP design (from Fig. 3) that does (PV). The impact of the local loop, although not completely apparent in the NPV closed-loop results, was quite large, resulting in heavy damping of the 10-, 17-, and 25-Hz modes. However, because the performance was dominated by the low-frequency response, primarily the 2.26- and 3.73-Hz modes, which were difficult to control without the rate gyro measurement, the overall NPV pointing error performance was 3.5 times worse than the best performance achieved by the FEM PP design (21.8 dB vs 31.0 dB). This performance degradation is to be expected given that the NPV controller does not use a direct measure of the performance metric. The asterisk in Fig. 7 indicates the controller was designed with the HAC/LAC method.

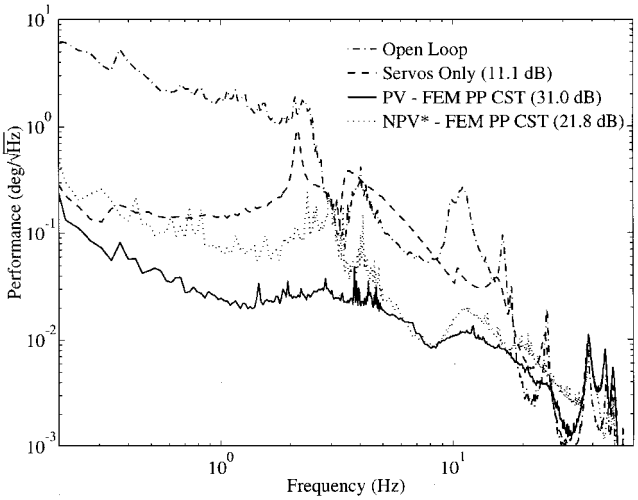

Fig. 7 Closed-loop performance results for configuration I showing degradation when the performance metric z is not fed back (NPV) as compared to the best FEM PP controller that utilizes z (PV). The * indicates that this controller was designed with the HAC/LAC method.

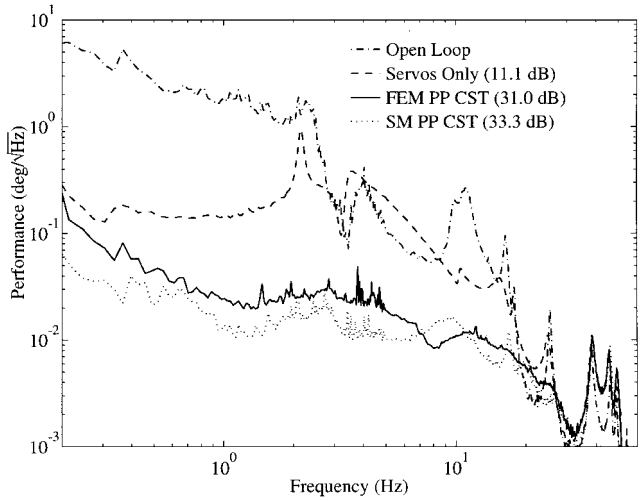

Fig. 8 Comparison of a shifted-model-based controller (SM PP) with an original FEM-based controller (FEM PP) on configuration I.

It is common in many systems that the PV cannot be directly fed back. These representative closed-loop results on MACE indicate that the achievable performance will degrade. However, the small set of results clearly shows that reasonable performance improvements and robustness can still be obtained using robust controllers that do not have direct access to the performance metric.

C. SM

A family of PP controllers was designed on configuration I using uncertainty model 2 (Table 3), which includes an SM and small parameter variations, as shown in Fig. 2. As discussed earlier, it is appropriate to use this approach if there is high confidence in the predicted uncertainty model. Because of the reduced size in uncertainty bounds about the shifted means, use of uncertainty model 2 in analysis and synthesis should result in higher authority controllers. Experimental performance will, however, depend more strongly on correct predictions of the mean variations in the error model (Table 3).

Figure 8 shows the results of two PP controllers. The FEM PP controller is the best PP controller using the FEM and uncertainty model 1 and is identical to that in Fig. 3. The SM PP result corresponds to the best PP controller using the FEM shifted by the predicted mean errors of the uncertainty model.[12,13] The SM PP controller performed 30% better than the best FEM PP controller. However, because higher authority FEM PP controllers were destabilized due to the unmodeled tether mode (and were not in the SM case), the results are inconclusive on whether this improvement of the SM PP performance was due to unmodeled dynamics, reduced conservatism, or both. However, comparisons between the SM and measured open-loop data do indicate that this form of the uncertainty model can be very useful for on-orbit control design.

IV. On-Orbit Configuration II Closed-Loop Experiments

Configuration II (the L shape) was used to investigate a set of hardware in 0-g that had only been tested on the ground in a different configuration, i.e., configuration I. This change in configuration was included in the MACE program to provide a strong test of the ability of the CSTs to model, predict, and account for significant variations in system dynamics. PP controllers were designed for configuration II using appropriate versions of the FEM, uncertainty model, and μ analysis. In addition, an MM was also developed on-orbit, and both FEM- and MM-based controllers were redesigned. The primary difference between the on-orbit operations for the two configurations was the extent of experiments and redesigns that were implemented.

A. Configuration II Results

The process of determining the analytical model of configuration II was different from that used for configuration I. Although the configuration I model was updated using ground test data, there

Table 4 Data showing the predicted 0-*g* uncertainty model for configuration II

Mode no.	f_{FEM}, Hz	Uncertainty model $\overline{\Delta f}$, %	Uncertainty model $\widehat{\Delta f}$, %	Data $\overline{\Delta f}$, %	Data $\widehat{\Delta f}$, %
1	2.45	0.0	4.8[a]	1.1	2.2
2	5.35	0.0	3.8[a]	3.1	1.9
3	8.41	0.0	6.4[a]	1.8	3.0
4	17.6	0.0	0.7[a]	−0.4	1.3
5	19.0	0.0	7.4[a]	−2.2	1.5
6	26.0	0.0	1.4[a]	−1.4	0.5
7	31.8	0.0	5.4	−12.4	0.5
8	37.0	0.0	1.1	−6.8	0.6
9	42.7	0.0	4.3	−5.3	2.3
10	49.9	0.0	3.5[a]	−3.5	2.8

[a]Mean data frequencies within predicted bounds: 7 of 10.

was no direct correlation with measured open-loop data possible prior to flight for configuration II. An alternative method had to be developed in which the updated parameters from the configuration I model were used as the starting point for configuration II. The differences between the two structural configurations were then included in the configuration II model. If the physical parameters of configuration I have been updated correctly during 1-*g* testing, then the resulting 0-*g* model for configuration II should be quite accurate. The configuration II 0-*g* model was used for 0-*g* identification experiment design, controller design, and performance prediction prior to flight. The relatively large changes in the modal frequencies from configuration I to configuration II are shown in Tables 2 and 3.

As shown in Ref. 9, the accuracy of the configuration II FEM and MM are comparable to that for configuration I. This was expected for the identification model, which was directly fit to the measured MIMO data. However, given the potential errors in the modeling process for configuration II, this level of accuracy was not necessarily expected for the FEM. The closeness of the FEM to the measured data for configuration II confirmed that a highly accurate model of a 0-*g* structural configuration that cannot be tested on the ground can be constructed from a similar configuration that was tested in 1 *g*.

As with the FEM, the configuration II uncertainty model was based on the configuration I uncertainty model, but with an added step linked to the rotation of the physical degrees of freedom of the L configuration. Details of this prediction are given in Ref. 27. Table 4 summarizes the uncertainty model for configuration II. Only the more conservative form of the uncertainty model is shown because no SM controllers were designed for this configuration. Of the 10 frequencies shown, 7 of the mean errors were predicted correctly. These results are quite good considering the uncertainty model development contains an additional step in the prediction process (configuration I to configuration II).

The closed-loop results for configuration II are shown in Figs. 9 and 10 (analogous to configuration I results in Fig. 3 and 4). Figure 9 shows the performance results for FEM designs with the nominal topology of the five rate gyros, three reaction wheels, and primary gimbal. The multiple model design method was used for these particular controllers. The solid line in Fig. 9 shows that the best FEM PP design (using μ analysis and uncertainty model in Table 4) achieved 28.0-dB improvement, with significant broadband disturbance rejection up to 20 Hz. It also shows, however, a lightly damped closed-loop resonance at 8.5 Hz, which was not predicted by the μ analysis, and a slight amplification in the 20–30 Hz range. The FEM RD controller (using open-loop data analysis) was designed to increase robustness of the FEM-based designs in the 8 and 20–30 Hz ranges. As shown in Fig. 9, these frequency ranges are much improved, but performance was sacrificed (26.9 dB).

Performance improvement of the best MM RD-based controller, shown in Fig. 10, is slightly worse than the FEM-based controllers up to 15 Hz. The 8-Hz amplification is much lower, however, and the 20–30 Hz region is better. Note also the slight amplification at 40 Hz, a result of robustness problems with the HAC. Overall, the higher authority FEM PP controllers achieved the best overall numerical performance. However, $\mathcal{H}_2$ performance alone is not necessarily the best measure of the closed-loop system response.

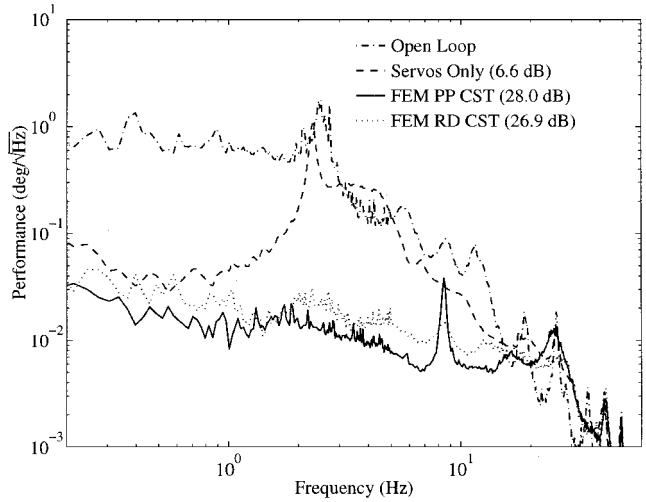

Fig. 9 On-orbit FEM-based results for MACE configuration II; predicted uncertainty model and μ-analysis used to test for robustness.

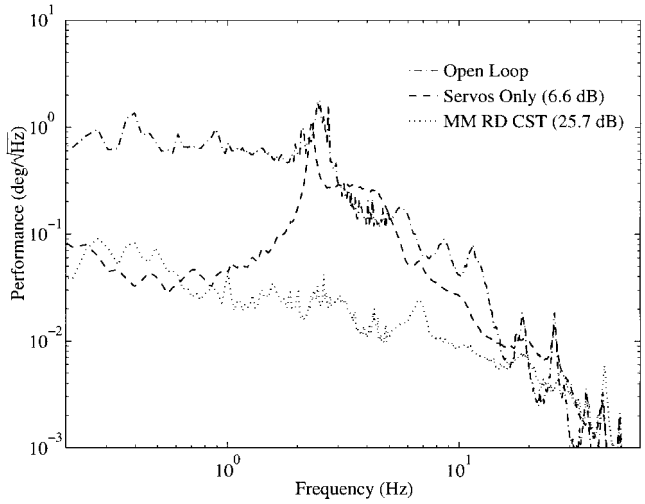

Fig. 10 On-orbit MM-based results for MACE configuration II; open-loop data analysis used to test for robustness.

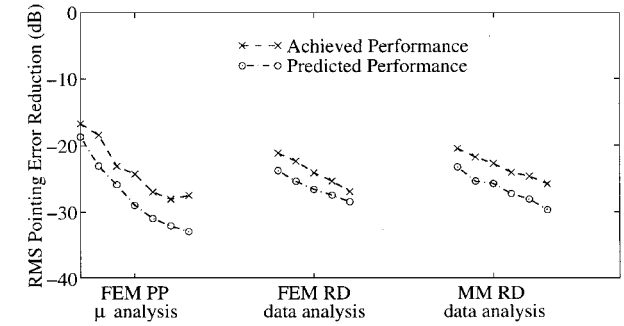

Fig. 11 Configuration II performance comparison.

The configuration II performance summary is shown in Fig. 11. As in Fig. 6, these curves show predicted and achieved performance for several families of controllers designed before (PP) or during (RD) the mission. The 8.5-Hz problem identified in Fig. 9 caused a divergence between the PP predicted and measured closed-loop responses. This divergence is even more dramatic than was seen for the configuration I PP controllers. In addition, the closed-loop performance of the last controller in the FEM PP family degraded significantly. The best PP design, which is the second-to-last controller in the FEM PP family, corresponds to FEM PP shown in Fig. 9, where the 8.5-Hz problem is already apparent.

With these PP performance results and the nonlinearity problems from configuration I already known, the emphasis for the

configuration II FEM RD controllers was to develop more robust controllers that avoided difficulties near 8.5 Hz and yielded more predictable results. As shown in Fig. 11, these objectives were partially achieved. The problems at 8.5 and 20–30 Hz have improved in the FEM RD controllers, but at the expense of approximately 1–2 dB in performance. Although this corresponds to only a small deterioration in performance, the equivalent design iteration for configuration I resulted in a 4-dB improvement. The FEM RD curve shows some disagreement between the predicted and achieved performance values, which is again a result of the 8.5-Hz problem. Unlike the PP case, however, these two curves do not diverge with increased control authority.

The measurement based configuration II controllers (MM RD) were designed after the problems on configuration I had been observed and partially resolved. Thus, similar problems were anticipated with the configuration II MM RD controllers because only one data set was available for this configuration at that point in the mission (when the controllers were designed). As a result, the MM RD controllers were designed very conservatively to avoid problems similar to the ones on configuration I. Figure 11 shows that performance improved within the family of the MM RD controllers, but did not achieve the performance levels of the FEM-based designs. In addition, there is a large discrepancy between the predicted and actual results caused by the use of only one data set for both the model generation and open-loop data analysis. The performance prediction discrepancy and the FEM performance surpassing the MM RD are consistent with the configuration I results.

B. Comparison of Configuration I and Configuration II Results

The objective of control design on configuration II of MACE was to determine the extent to which ground testing of an alternate configuration for a structure would aid in obtaining reliable control performance on a structure that could not be tested in 1 g. From this perspective, configuration II can be viewed as the primary space structure for which good closed-loop control is required. Configuration I corresponds to a simple, reasonably similar structure that could be cheaply built and tested on the ground. In light of this objective, the most important results for configuration II are the first family of PP control designs. It is this family of control designs that relied entirely on knowledge from the ground testing of the simpler alternative (configuration I) and modeling of the actual structure (configuration II). As such, the following comparison concentrates on the results of the PP controllers for these two configurations.

The FEM PP family of controllers for configuration I in Fig. 6 shows results obtained from a structure that was rigorously tested on the ground and then flown on-orbit. In comparison, FEM PP controllers for configuration II in Fig. 11 show results obtained for a structure that has never been tested on the ground, but shares the structural heritage of a system that has been tested extensively. The goal of control designs for each configuration was similar. Predicted performance in each of these plots shows a family of controllers increasing in expected performance from about 20 dB to over 30 dB. As shown in the two graphs, the achieved performance is also quite similar. Furthermore, in both configurations, the achieved performance for the lowest authority controller is close to the predicted value ($<$20 dB). For both configurations, the gap between the predicted and achieved performance increases for higher authority controllers. This trend demonstrates that, in both cases, the higher authority controllers tend to accentuate differences between the control design model and the actual structure. It is clear that the performance gap is larger for configuration II than for configuration I. This performance reduction is primarily due to the lack of ground testing with this exact configuration and clearly shows that ground testing is an essential part of control system design for high-performance space applications. However, Fig. 11 shows that the overall performance on configuration II was nearly 30 dB. This result clearly demonstrates that good performance can still be achieved if the ground testing is not performed on exactly the same structure, but instead on a similar structure that may be easier and cheaper to test on the ground. Thus, these comparisons provide some good insights on the important role that ground testing played in the configuration II results.

In summary, the good results obtained on configuration II do not imply that ground testing is an unnecessary step in control design for space applications. On the contrary, configuration II control design models and selection of performance weights were very heavily dependent on parameters obtained from ground testing of configuration I. In fact, it was the ground testing of configuration I that enabled accurate modeling and effective PP control of configuration II. These results show that even if the actual structure cannot be ground tested, useful information can be obtained by using a similar structure that can be tested on the ground.

V. Conclusions

The objective of this paper was to present an in-depth analysis of the extensive closed-loop results from the on-orbit operations of MACE. The nominal straight configuration for MACE, which was tested on the ground, was used to demonstrate excellent performance improvement using both PP (31.0 dB) and RD (35.2 dB) controllers. The MM-based redesigns, however, did not perform as well (33.0 dB) primarily because of a lack of design heritage and the errors associated with the identification of a system that contains nonlinearities. Similar levels of performance were achieved on a second L configuration that was not tested on the ground prior to flight. These results clearly showed the benefits of ground testing the system, even if it must be tested in a different configuration than it will be used in operation. In summary, the MACE mission 1) successfully demonstrated that robust control techniques can be used to design controllers that achieve good on-orbit performance based on predicted models of the dynamics and the errors in these dynamics, 2) confirmed that this performance can be improved and made more predictable using an on-orbit redesign sequence based on analysis with measured on-orbit data and control design based on the refined or identified on-orbit dynamic, 3) demonstrated that techniques and design procedures developed as part of the CST can be used to develop controllers for a configuration of the system that had never before been tested on the ground, and 4) demonstrated that good performance improvement can still be achieved when the performance metric is not directly fed back.

In conclusion, these results summarize a very successful investigation of control design issues associated with a contemporary solution to the CSI problem. It is now hoped that these experimental on-orbit results, combined with the extensive ground-based tests that have already been published, will improve the confidence in these advanced analysis and synthesis techniques so that they will be applied to future spacecraft that cannot be tested on the ground in a sufficiently realistic 0-g environment.

Acknowledgments

This work was supported by the NASA IN-STEP Program and NASA Langley Research Center Controlled Structures Interaction (CSI) Office with Gregory Stover and Jerry Newsom as Contract Monitors, under Contracts NAS1-18690 and NAS1-19622.

References

[1]Wie, B., Horta, L., and Sulla, J., "Active Structural Control Design and Experiment for the Mini-MAST," *Proceedings, American Control Conference* (San Diego, CA), Inst. of Electrical and Electronics Engineers, Piscataway, NJ, 1990, pp. 1428–1434.

[2]Collins, E. G., Jr., King, J. A., and Hyland, D. C., "High Performance, Accelerometer-Based Control of the Mini-MAST Structure," *Journal of Guidance, Control, and Dynamics*, Vol. 15, No. 4, 1992, pp. 885–892.

[3]Balas, G. J., Young, P., and Doyle, J. C., "The Process of Control Design for the NASA Langley Minimast Structure," *Proceedings, American Control Conference* (Boston, MA), Inst. of Electrical and Electronics Engineers, Piscataway, NJ, 1991, pp. 562–567.

[4]Smith, R. S., Chu, C.-C., and Fanson, J. L., "The Design of $\mathcal{H}_\infty$ Controllers for an Experimental Non-Collocated Flexible Structure Problem," *IEEE Transactions on Control Systems Technology*, Vol. 2, No. 2, 1994, pp. 101–109.

[5]Sparks, D. W., and Juang, J.-N., "Survey of Experiments and Experimental Facilities for Control of Flexible Structures," *Journal of Guidance, Control, and Dynamics*, Vol. 15, No. 4, 1992, pp. 801–816.

[6]Hyland, D. C., Junkins, J. L., and Longman, R. W., "Active Control Technology for Large Space Structures," *Journal of Guidance, Control, and Dynamics*, Vol. 16, No. 5, 1993, pp. 801–821.

[7]Miller, D. W., How, J. P., Campbell, M., Grocott, S. C. O., Glaese, R., Liu, K., and Tuttle, T., "Flight Results from the Middeck Active Control Experiment (MACE)," *AIAA Journal*, Vol. 36, No. 3, 1998, pp. 432–440.

[8]Miller, D., Saarmaa, E., and Jacques, R., "Preliminary Structural Control Results from the Middeck Active Control Experiment (MACE)," *Proceedings, AIAA Dynamics Specialist Conference* (Dallas, TX), AIAA, Washington, DC, 1992, pp. 566–576 (AIAA Paper 92-2138, April 1992).

[9]Glaese, R., and Liu, K., "On-Orbit Modeling and System Identification for MACE," *Proceedings of IFAC 13th World Congress* (San Francisco, CA), Vol. D, Elsevier Science, Oxford, England, UK, 1996, pp. 37–42.

[10]Grocott, S. C. O., How, J. P., and Miller, D. W., "Experimental Comparison of Robust $\mathcal{H}_2$ Control Techniques for Uncertain Structural Systems," *Journal of Guidance, Control, and Dynamics*, Vol. 20, No. 3, 1997, pp. 611–613.

[11]Grocott, S. C. O., How, J. P., Miller, D. W., MacMartin, D. G., and Liu, K., "Robust Control Design and Implementation on the Middeck Active Control Experiment (MACE)," *Journal of Guidance, Control, and Dynamics*, Vol. 17, No. 6, 1994, pp. 1163–1170.

[12]Campbell, M. E., Grocott, S. C. O., How, J. P., Miller, D. W., and Crawley, E. F., "Verification Procedure for On-Orbit Controllers for the Middeck Active Control Experiment," *Proceedings, 1995 American Control Conference* (Seattle, WA), Inst. of Electrical and Electronics Engineers, Piscataway, NJ, 1995, pp. 3600–3605.

[13]Grocott, S. C. O., and Campbell, M. E., "Control Analysis Results for MACE: Methods and Limitations," *Proceedings of IFAC 13th World Congress* (San Francisco, CA), Vol. D, Elsevier Science, Oxford, England, UK, 1996, pp. 43–48.

[14]Young, P. M., Newlin, M. P., and Doyle, J. C., "μ Analysis with Real Parametric Uncertainty," *Proceedings, IEEE Conference on Decision and Control* (Brighton, England, UK), Inst. of Electrical and Electronics Engineers, New York, 1991, pp. 1251–1256.

[15]Balas, G. J., and Young, P. M., "Control Design for Variations in Structural Natural Ferquencies," *Journal of Guidance, Control, and Dynamics*, Vol. 18, No. 2, 1995, pp. 325–332.

[16]Sesak, J. R., "Sensitivity Constrained Linear Optimal Control Analysis and Synthesis," Ph.D. Thesis, Univ. of Wisconsin, Madison, WI, 1974.

[17]Hyland, D. C., "Maximum Entropy Stochastic Approach to Controller Design for Uncertain Structural Systems," *Proceedings, American Control Conference* (Arlington, VA), Inst. of Electrical and Electronics Engineers, Piscataway, NJ, 1982, pp. 680–688.

[18]Grocott, S. C. O., MacMartin, D. G., and Miller, D. W., "Experimental Implementation of a Multi-Model Design Technique for Robust Control of the MACE Test Article," *Proceedings, Third International Conference on Adaptive Structures* (San Diego, CA), Technomic, Lancaster, PA, 1992, pp. 375–387.

[19]How, J. P., Hall, S. R., and Haddad, W. M., "Robust Controllers for the Middeck Active Control Experiment Using Popov Controller Synthesis," *IEEE Transactions on Control Systems Technology*, Vol. 2, No. 2, 1994, pp. 73–87.

[20]Doyle, J. C., "Structured Uncertainty in Control System Design," *Proceedings, IEEE Conference on Decision and Control* (Ft. Lauderdale, FL), Inst. of Electrical and Electronics Engineers, New York, 1985, pp. 260–265.

[21]Campbell, M. E., and Crawley, E. F., "Classically Rationalized Low-Order Robust Structural Controllers," *Journal of Guidance, Control, and Dynamics*, Vol. 21, No. 2, 1998, pp. 296–306.

[22]Kwakernaak, H., and Sivan, R., *Linear Optimal Control Systems*, Wiley-Interscience, New York, 1972, Chap. 5.

[23]How, J. P., Glaese, R. M., Grocott, S. C. O., and Miller, D. W., "Finite Element Model Based Robust Controllers for the MIT Middeck Active Control Experiment (MACE)," *IEEE Transactions on Control Systems Technology*, Vol. 5, No. 1, 1997, pp. 110–118.

[24]Safonov, M., and Tsao, T., "The Unfalsified Control Concept: A Direct Path from the Experiment to the Controller," *Proceedings, Conference on Feedback Control, Nonlinear Systems, and Complexity*, Springer–Verlag, London, 1994, pp. 196–214.

[25]Kosut, R. L., "Uncertainty Model Unfalsification: A System Identification Paradigm Compatible with Robust Control Design," *Proceedings, 34th IEEE Conference on Decision and Control*, Inst. of Electrical and Electronics Engineers, New York, 1995, pp. 3492–3497.

[26]Aubrun, J.-N., "Theory of the Control of Structures by Low-Authority Controllers," *Journal of Guidance and Control*, Vol. 3, No. 5, 1980, pp. 444–451.

[27]Campbell, M. E., and Crawley, E. F., "Development of Structural Uncertainty Models," *Journal of Guidance, Control, and Dynamics*, Vol. 20, No. 5, 1997, pp. 841–849.